We are IntechOpen, the world's leading publisher of Open Access books
Built by scientists, for scientists

5,300
Open access books available

130,000
International authors and editors

155M
Downloads

154
Countries delivered to

Our authors are among the

TOP 1%
most cited scientists

12.2%
Contributors from top 500 universities

BOOK CITATION INDEX
CLARIVATE ANALYTICS
INDEXED

WEB OF SCIENCE™

Selection of our books indexed in the Book Citation Index
in Web of Science™ Core Collection (BKCI)

Interested in publishing with us?
Contact book.department@intechopen.com

State of the Art of Magnetic Gears, their Design, and Characteristics with Respect to EV Application

Daniel Fodorean

Additional information is available at the end of the chapter

Abstract

This chapter briefly explains the advantage of using magnetic gears (MGs) for transportation applications. Usually, a traction EV unit consists of, besides the engine or motor, a mechanical gear. The drawbacks of using mechanical gears have been emphasized, especially with respect to high-speed motorization, where high transmission ratio can be reached only by connecting multiple gears in series. A magnetic gear is capable of overcoming these issues. The chapter presents a state of the art on the available MGs, with fixed or variable transmission ratio, pointing out their applicability. Next, the possible design approaches (harmonic, magnetic reluctance equivalent circuit, and vector potential) are introduced. Furthermore, the output performances (power and torque) of two types of studied MGs are evaluated, with emphasis on the main loss criteria: iron losses in all the active parts of the MG. Finally, the influence of several materials is observed by means of numerical computation in order to decide, based on specific configuration, the most suited variant for transportation and aeronautic applications.

Keywords: EV application, state of the art of magnetic gears, design, FEM numerical computation, iron loss

1. Introduction

Electric vehicles (EVs) offer promising solutions for sustainable transport, but their development is hampered by a number of technological challenges [1–10]. To be competitive with internal combustion engines, EVs must offer the same dynamics, range, comfort conditions, and be cost effective [1, 2].

Since 2012, there has been an increase in the number of electric cars running on highways [3, 6, 8]. Most of them are powered by permanent magnet synchronous machines (PMSM)—due to their high energy from rare earths materials used for excitation—and sometimes by DC motors (DCM), for Renault ZOE model, induction machines (IM), or Tesla-S model. **Table 1** presents few of the best-selling electric cars, in series production, with some technical characteristics and their cost/unit. Apart from Tesla-S model, which is extremely expensive, car manufacturers are generally proposing motorization variants with approximately the same performance and features. The best sold model today is the Nissan Leaf, launched in December 2010; by December 2016, it should reach over 200,000 units sold globally. Among European variants, Renault-Zoe and BMW-i3 are the bestsellers, noting that the German car manufacturer entered the market in the autumn of 2013 and by the end of this year, 2016, it should surpass 60,000 sold-ordered units. The number of electric units sold (globally surpassed the amount of 1 million units) is far from the number of internal combustion engine variants sold, one reason being the cost, in addition to the issue of autonomy. Basically, because of reduced autonomy and the reduced number of electric cars sold, the production cost/unit for EVs is high. Nevertheless, the trend is clear and with the increase in the number of supplying stations, the number of electric cars sold should increase exponentially.

Model	EM	EM power	Top speed	Autonomy	Other characteristics and price
Renault ZOE	DCM	43/65 kW	135 km/h	100 km	22 kWh/400 V Li-I battery; **27k€**;
Citroen C-ZEROs	PMSM	47 kW	130 km/h	100 km	Li-I battery; **30€**;
Peugeot iOn	PMSM	47 kW	130 km/h	100 km	Li-I battery; 0–100km/h:16s; **30k€**
Nissan Leaf	PMSM	80 kW	150 km/h	121 km	24 kWch Li-Manganate battery; **29k$**;
BMW-i3	PMSM	65 kW	150 km/h	130 km	360 V Li-I battery; 0–60 km/h:< 4 s; **41k$**;
Smart electric	PMSM	35 kW	125 km/h	145 km	Li-I battery; 0–60 km/h: 4.8 s; **20k$**
Mitsubishi i-MiEV	PMSM	49 kW	130 km/h	100 km	16 kW/330 V Li-I battery; **34k$**
Tesla S	IM	225 kW	193 km/h	335 km	60 kWh battery; 0–100km/h:<6s; **71k$**

Table 1. Some of the best-selling electric cars, in series production: propulsion's characteristics and approximate cost/unit.

An interesting perspective was presented by the EVIG institute in 2013, see **Figure 1**. In their estimation, at the end of 2016 the number of cars sold should reach 2 million, and by the end of 2020 we should expect to have about 6 million electric cars running on streets. It looks promising, and we need to leave it to time to confirm their estimation.

The autonomy range of electric cars is affected by the load capacity and the energy storage capability, which is directly influenced by the total weight of the car and the propulsion's efficiency [2]. Thus, a closer look at the propulsion system should be considered.

The components of the drive chain are the electrical propulsion (electrical machine and transmission), the converter, and the battery—the energy flow within the system's components

is bidirectional. The largest share of losses is in the electrical propulsion, 72%, on the static converter the loss is about 19%, and at the battery level the loss is about 9% (**Figure 2**).
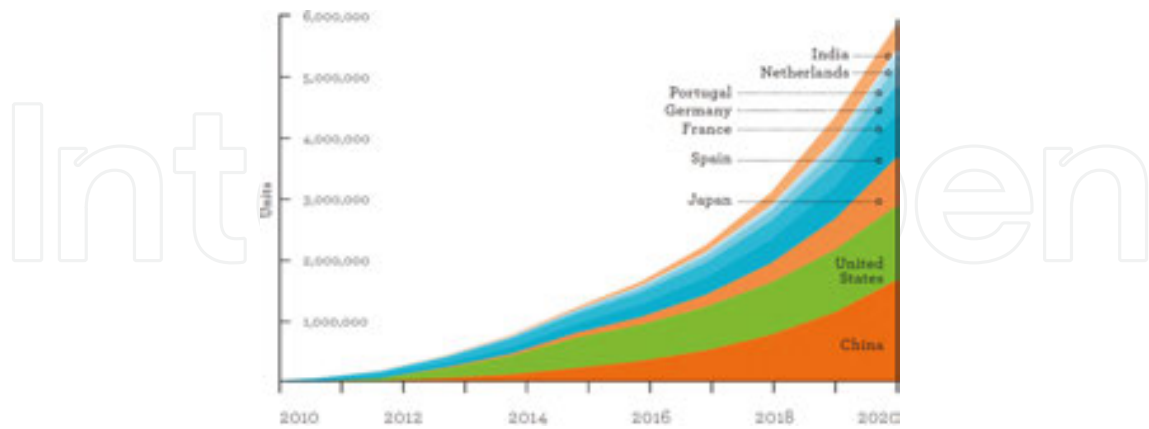

Figure 1. Perspective on the sold electric cars, worldwide.
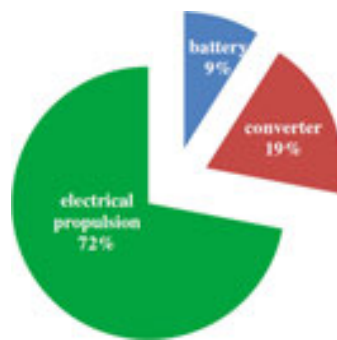

Figure 2. Losses in the propulsion system.

Therefore, acting mainly on the electrical propulsion by improving its efficiency and power density will improve the overall autonomy of the EV [3–5].

With regard to the existing propulsion solution, it can be seen that over time, the operating speed has substantially increased [11–19]. As an example, let us take a look at few series-manufactured cars: if in 2003, the electric motor of the Toyota-Prius-Hybrid was at 6000 r/min, the latest model is running at 12,000 r/min [9]; for the BMW-i3 model, the nominal speed is 4000 r/min, while the maximum speed (in flux-weakening operating conditions) is 11,800 r/min; for the present Mitsubishi-iMiev model, the speed of the motor is 9000 r/min. We can conclude that all car manufacturers are looking at increasing the speed of motorization, having in mind the improvisation of power density of the traction chain, as well as EV's autonomy.

In this context, we should recall that higher speeds are not easily and efficiently possible, since attached to the electric motor a gear is placed in order to transfer the torque-speed to the car's traction wheels. For a tire diameter of about 0.6 m and a circumferential speed of 1500 r/min coming from the gear, the vehicle's traveling speed is 47 m/s, meaning 169 km/h. In such a

case, even if we would like to increase the speed of the propulsion motor, a classic mechanical gear with high transmission ratio is difficult to obtain; usually, we consider cascaded gear units, but this will affect the global power density of the traction system and its efficiency. Thus, a solution is needed to overcome this drawback. In this context, the use of a magnetic gear (MG) could be the right solution.

In **Table 2**, a weight comparison of the possible motorization solutions is presented, based on personal experience or technical data found on the available equipment.

Component	Electric propulsion		
	Classic (low speed) with mechanical gear	**High speed (26000 r/min, water cooled) with mechanical gear in steps**	**High speed (26000 r/min, water cooled), magnetic gear with 1 fix step**
Motorization (30 kW)	130 kg	16 kg	16 kg
Gear	≈50 kg	≈80 kg	33 kg
Converter (30 kW/water cooled)		≈8 kg	
Battery (380 Vcc, 18 kWh)		≈200 kg	
Total weight	**≈388 kg**	**≈304 kg**	**≈257 kg**
Remarks	Increased volume and weight, acceptable efficiency	Decreased volume and weight, efficiency affected by the gear in steps	Reduced volume and weight, increased efficiency, limitation for wide-speed operation

Table 2. Comparison of traction chain weights for different configurations containing classic or magnetic gears.

For the sake of comparison, we have considered three possible variants: one motorization with 6500 r/min, another one with high-speed motor (running at 26,000 r/min), while the traction is used with a fixed mechanical gear ratio, or with multilevel gear (to reach the desired ratio), or when, for the same high-speed machine, we have a magnetic gear (MG) excited with rare earth material. **Table 2** shows how for the same converter and battery pack, high-speed motorization has a reduced weight with about 80 kg (with fixed mechanical gear). Otherwise, when using an MG with high transmission ratio, the performance and power density are high, while the weight of the entire propulsion system is decreased by about 130 kg—which is a huge win for an EV.

The detailed structure of a magnetic gear will be presented in the next section. Here, we should recall that the main materials found on a magnetic gear are the permanent magnet for excitation, and the steel. Thus, the MG has one important disadvantage: it is extremely expensive because the excitation (on both rotating parts—the low-speed rotors—which are interacting for the production of the torque) is generally made of Nd-Fe-B. According to **Table 3**, at the present time, the most important rare earth resources are found in Asia, particularly in China; even the European production is under Hitachi license—meaning that it is again an Asian license. Due to the monopoly imposed by Asian countries, the price of this type of

material reached 130 €/kg in 2010–2011 (from 50 €/kg in 2002), now being stabilized after a slight decrease at 100–110 €/kg. As a consequence, the European and other countries are trying to avoid this monopoly. Moreover, the global earth resources in terms of rare earth materials cannot cover today's industry needs.

Nd-Fe-B worldwide production, in 2013	×1000 (Tons)	%
China	70	~80
Japan	17	~19
EU	1.5	~1
Total	88.5	100

Table 3. Worldwide production of Nd-Fe-B at the 2013-year level.

As a result, an important decision was first taken in 2012, when the European Research Agency (ERA) said that it will not fund research projects that use rare earth materials, such as Nd-Fe-B or Sm-Co type; it is for this reason that research institutes and universities have lately reconsidered the use of ferrite material (5 €/kg) or the possibility to avoid any excitation material, by means of passive rotors, such as reluctance synchronous machines (RSM). Some others are trying to reduce the volume of rare earth materials, calling such machines as PM-assisted ones.

Otherwise, from previous research experience and information found in the literature, it has been observed that a magnetic gear with specific configuration of poles/teeth will induce specific torque ripples in the propulsion system [25–31]. Thus, when thinking of an MG, we are interested in finding an appropriate configuration which produces the lowest vibration and noise level. These elements will be considered with respect to the MG topic, while considering it for the EV application.

2. Principal of operation of magnetic gears, available topologies, and design approaches

A classic gear, meaning a mechanical one, which relies on the contact of two wheels with different number of iron teeth (see **Figure 3** left), has some important drawbacks. First of all, physical contact is needed, which involves local friction and heat (and consequently losses). Besides, lubrication is needed from time to time, in appropriate quantity. Moreover, the teeth are physically and irreversibly damaged with time due to material friction and fatigue. Thus, the losses increase after several hours/years of operation. All these disadvantages are eliminated in the case of a magnetic gear (MG). Above all, another important benefit of MG use should be indicated here: in order to obtain high transmission ratio, one should use complex gears, with more than two integrated wheels. Usually, two or more mechanical gears are cascaded (linked) in the transmission chain. Such configurations drastically affect the power

density and the efficiency of mechanical transmission. This is not the case for MGs: the most important amount of loss is found in the iron loss component, while the mechanical one (due to friction with the air and on the bearings) is in the same range as that of mechanical gears.
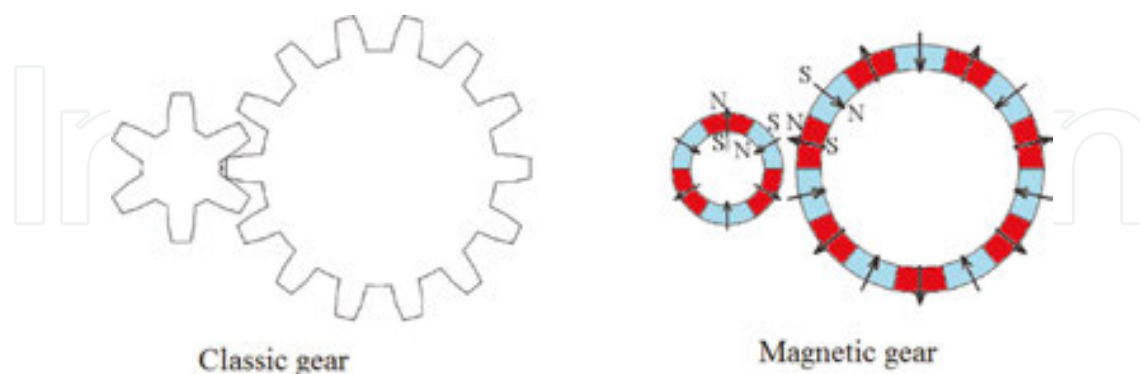

Figure 3. The classical (left) and magnetic (right) gears.

The first reference of a gear without mechanical contact dates back to 1916 [20, 34]. Since then, the benefits of MG were highlighted, namely: no need for lubrication, no local heating (no friction losses), and no risk of breaking the elements used to transfer power [20–41]. However, the first built viable solution dates to the 1980s (see a similar configuration of such an MG in **Figure 3** right)—evaluated from the torque capability point of view in [35]—but its efficiency was somewhere in the 25–30% range (only a part of magnetic poles was in active magnetic contact). The first efficient MG solution that fully exploits all the gear magnets dates back to early 2000 [20]—see **Figure 4**. Numerous other configurations of MGs have been proposed with time [21–41]. Some of these variants will be shown here in order to have a clue about the state of the art, but before that, we will see the principal of operation of a regular MG.
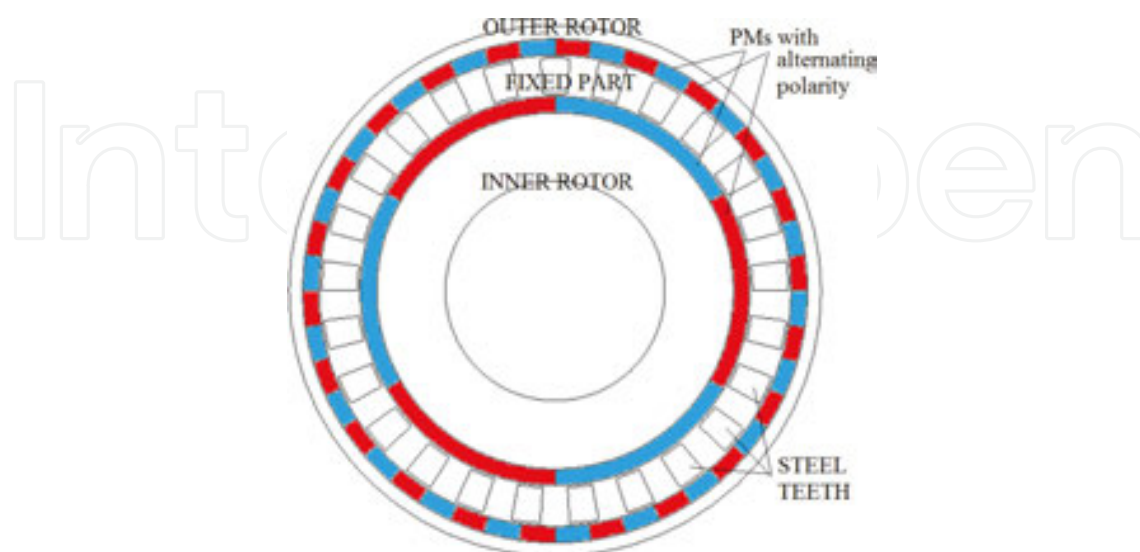

Figure 4. Cross section of the main elements of the active parts of an efficient MG.

2.1. Principal of operation

The operation of the MG is based on the modulation of the magnetic field created by the rotating magnetic poles of the high-speed rotor within the iron poles of the static part [20, 33]. The main components of such MG are shown in **Figure 4**. The field developed in the static iron will interact with the field created by the magnetic poles of the low-speed (outer) rotor and will force it to run in the opposite direction [20, 33].

It has been shown that the highest torque transmission is obtained with the following equality [20]:

$$p_{out} = N_s - p_{in} \tag{1}$$

where p_{in}, N_s, and p_{out} are the number of poles pair for the inner (high-speed) rotor, of the fixed iron part and of the outer (low-speed) rotor, respectively. The correspondences between the output (ω_{out}) and input (ω_{in}) speed and the gear ratio (*gr*) are:

$$\omega_{out} = -gr \cdot \omega_{in} \tag{2}$$

$$gr = -\frac{\omega_{out}}{\omega_{in}} = \frac{p_{in}}{p_{out}} \tag{3}$$

Besides, with a specific configuration of the MG, it is possible to obtain smooth mechanical characteristics—the lowest possible torque ripples are obtained if the ripples coefficient (k_r) equals unity (the ideal case) [33].

$$k_r = \frac{2 \cdot p_{in} \cdot N_s}{LCM(2 \cdot p_{in}, N_s)} \tag{4}$$

where *LCM* denotes the 'least common multiple' between the number of poles of the inner rotor and the fixed iron teeth.

These are just a few elements showing the operating principle of an MG in general. The analytical modeling of different MGs found in the literature will be summarized later, after the presentation of a detailed state of the art on the existent configurations.

2.2. State of the art of magnetic gears with fixed or variable transmission ratio

The first efficient MG, having radial configuration, was proposed by Attalah [20]. Next, other variants have been proposed. For example, in [34] a concentrated flux variant (or the so-called *spoke configuration*) was considered for the inner (high-speed) rotor; for the low-speed and high-torque rotor, the surface-mounted variant is almost exclusively used—because the surface-

mounted topology proposes the best power density, and because at low speed the risk of magnet's detaching is reduced. Such a topology, like the one presented in [34], is shown in **Figure 5**. This variant is again of radial flux. Thus, one could imagine all types of configurations for the high-speed rotor, which are usually used for classic permanent magnet synchronous machines (PMSM)—see different rotor configurations in **Figure 6**.
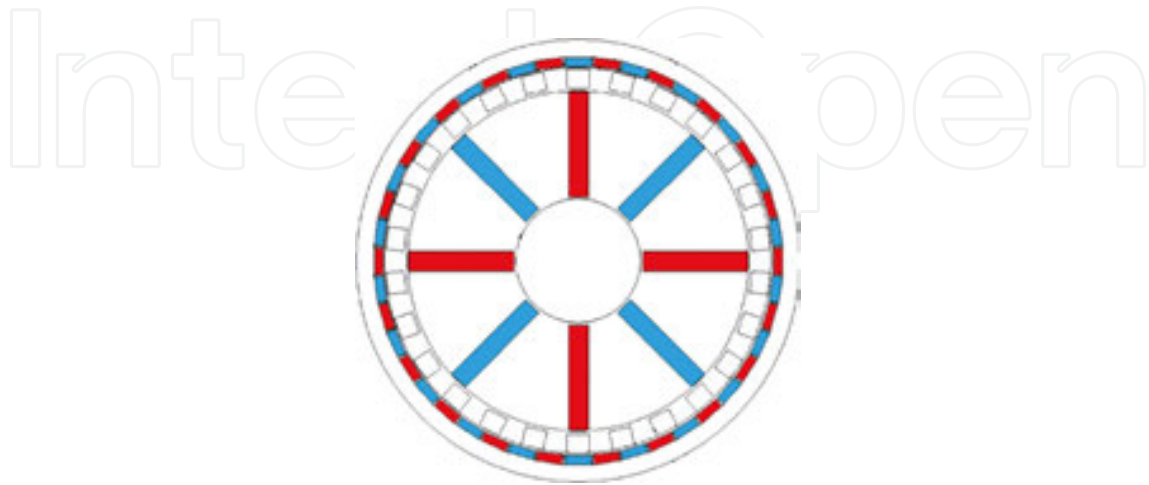

Figure 5. Cross section of flux-concentrated MG (spoke variant for the high speed rotor).
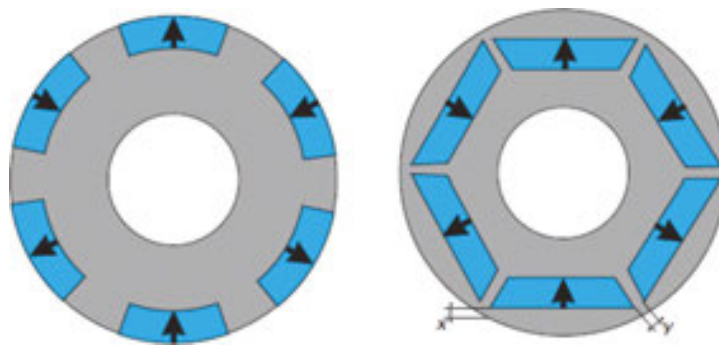

Figure 6. Possible rotor configurations for the radial flux MG: partially inset (left) and buried magnet (right) variants.

Since in an MG we are not interested in the flux-weakening capabilities of the structure itself, the structure with surface-mounted magnets based on Nd-Fe-B material on the high-speed rotor (shown in **Figure 4**) is almost exclusively used. When cheaper magnet material such as the ferrite is used, the concentrated flux (or spoke) variant can be considered (**Figure 5**). The partially or entirely inset magnet variants in **Figure 6** could be appropriate solutions when very high speeds are to be considered, in order to avoid the use of a consolidating ring of carbon or Titan material—which increases the air gap of the MG and drastically reduces its capability of producing the torque.

Axial flux variants [28, 29], such as the ones shown in **Figure 7**, have also been analyzed, since the axial configuration offers the best power density (due to reduced volume and weight on the passive elements: shaft and housing).
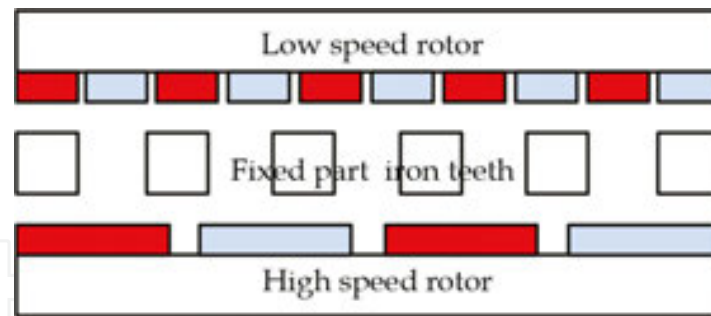
Figure 7. Axial flux MG configuration.

Usually, the MG is attached at the inner rotor side to an electric motor, to transfer the desired speed and torque to a load. In order to reduce the passive elements, some researchers have proposed integrated configurations. Such configurations are usually built on in-wheel motor variants, meaning that the motor has an inner stator and an outer rotor. Next, attached to the outer rotor is the inner rotor of the MG above, the static part with iron teeth, and on top of it the second rotor of the MG. Such compact variants have been studied in [26, 30, 31, 39, 40]. The transition from in-wheel motor to integrated MG-motor is shown in **Figure 8**.
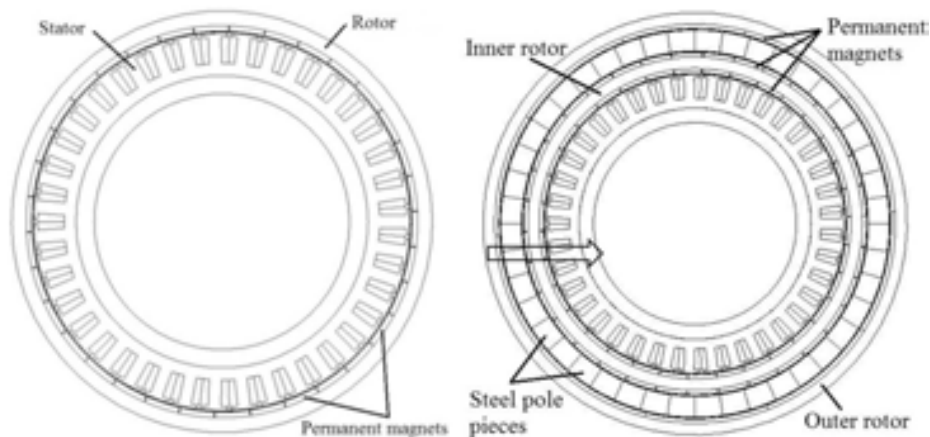

Figure 8. Transition from in-wheel motor to integrated MG-motor configuration [40].

Other types of MGs, such as the cycloid [27] and even the ones with variable transmission ratio [24, 29] have been proposed. Thus, we can emphasize that this topic is of real interest in the field of EVs (for the majority of applications) and power generation for wind turbines [39]. Next, the reader's attention will be focused on the existent analytical approaches that can be used for MG's design and modeling.

2.3. Analytical approaches for the design of MGs

There are three main design techniques for the analytical modeling of magnetic gears, similar to the case of electrical machines: the harmonic approach [25, 27, 30, 36], the magnetic reluctance equivalent circuit [22, 38], and vector potential algorithm [26, 28, 37, 41].

2.3.1. Analytical design of MG through harmonic approach

For the solution presented in [20], later we had the formularization of the operating principal, given by Atallah [36] and others [25, 27 , 30]. In order to express the torque produced by the two rotors rotating in opposite direction, we first need to express the flux density in the air gap. This flux density has two components: a radial and a tangential one. Also, the influence of the stationary part (the iron teeth) has to be evaluated as a modulating component.

The two components of flux density, the radial and tangential one, produced by the inner rotor of the MG, are:

$$\begin{cases} B_{rin} = \sum_{n=1,3,5}^{\infty} a_n \cdot \cos(n \cdot p_{in} \cdot (\theta - \omega_{in} \cdot t + \alpha_0)) \\ B_{tin} = \sum_{n=1,3,5}^{\infty} b_n \cdot \sin(n \cdot p_{in} \cdot (\theta - \omega_{in} \cdot t + \alpha_0)) \end{cases} \tag{5}$$

where a_n, b_n, and α_0 are the Fourier coefficients and the initial shift angle of the rotor. Next, the modulating component of the fixed iron teeth, similarly obtained, is function of Fourier coefficients and initial shift angle of this armature, meaning a_n, b_n, and α_0:

$$\chi = c_0 + \sum_{m=1}^{\infty} c_m \cdot \cos(m \cdot N_s \cdot (\theta + \beta_0)) \tag{6}$$

Similar to (5), one can get the flux density components to the outer rotor of the MG. In [30] some detailed formulation was given for the harmonic components with the pole pair number equal to $(n \cdot p_{in})$ and $(m \cdot N_s - n \cdot p_{out})$, or equal to $(n \cdot p_{out})$ and $(m \cdot N_s - n \cdot p_{in})$.

The torque produced by the inner and outer rotor is a function of the pull-out torque, T_{min} and T_{mout} (γ_0 is the shift angle of the outer rotor of the MG) [30]:

$$\begin{cases} T_{in} = T_{min} \cdot \sin\left(\dfrac{N_s \cdot \beta_0 - p_{out} \cdot \gamma_0 - p_{in} \cdot \alpha_0}{p_{in}} \right) \\ T_{out} = T_{mout} \cdot \sin\left(\dfrac{N_s \cdot \beta_0 - p_{out} \cdot \gamma_0 - p_{in} \cdot \alpha_0}{p_{out}} \right) \end{cases} \tag{7}$$

2.3.2. Analytical design of MG through magnetic reluctance equivalent circuit

Based on the literature research, we have found a first approach on MG modeling through magnetic reluctance equivalent circuit in [22]. This approach is interesting because it also takes into account the steel material characteristic (through curve fitting). Actually, this paper was an adaptation of the method presented in [38] where the analytical design approach was applied to a brushless permanent magnet machine.

The method consists in computing the torque, as a function of a flux (Ψ_m) and magneto-motive force (F_m) product, produced in each element of the equivalent circuit. Such a magnetic reluctance equivalent circuit is shown in **Figure 9**.

$$T = \frac{n_\theta}{2 \cdot \pi} \cdot \sum_{j=1}^{n_\theta} \Psi_{mj} \times \Delta F_{mj} \tag{8}$$

where n_θ is the number of elements of reluctances on the considered equivalent circuit.
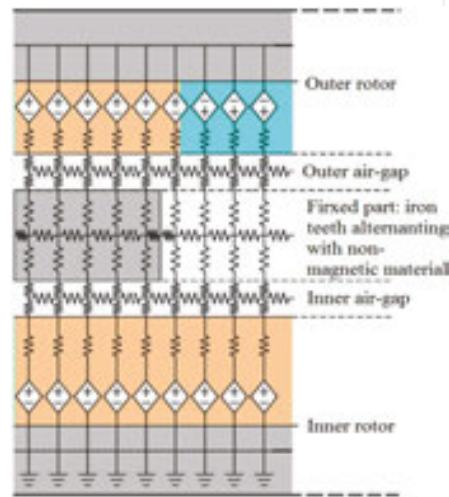

Figure 9. Magnetic reluctance equivalent circuit for MG design [22].

The magnetic flux is a function of the magnetic reluctance, which can be expressed through curve fitting for each specific material. For a certain iron sheet, the magnetic reluctance can be expressed as:

$$R(\Psi_m) = a_1 \cdot \frac{h}{S^1} \cdot \Psi^0 + a_n \cdot \frac{h}{S^n} \cdot \Psi^{n-1} \tag{9}$$

where h is the length of the flux for a specific trajectory and the S is the area of the flux on a specific element of the geometry—a or n index varies the function of material. These reluctances (and finally the fluxes) are calculated on radial and tangential direction.

The magneto-motive force, F_m, can be computed as well on each specific element, recalling that:

$$F_m = H_m \cdot h \tag{10}$$

where H_m is the magnetic field intensity calculated on each element of the magnetic circuit.

2.3.3. Analytical design of MGs through vector potential algorithm

The vector potential expressions, in both air gaps of the MG, have been detailed for radial and axial flux topologies in [28, 41]. Since the mathematical modeling for such an approach is quite laborious and goes beyond the scope of this state-of-the-art presentation of MGs, it will not be presented here. (It's worth mentioning that even the integral coefficients are detailed in the previous references; thus, the reader can investigate this topic if needed.)

With this, we have concluded a short presentation on the available analytical models used in the design of process of MGs. Next, we will consider two of the available configurations to evaluate their performances (in terms of iron loss and torque) and we will rapidly investigate the influence of certain materials used in the construction of MGs.

3. Characteristics of MGs with respect to their use in EV application

Two of the previously presented MG variants will be investigated here: the first one is an integrated motor-gear variant having an in-wheel configuration for the electric motor, and the second MG will be a high-speed variant with buried permanent magnets. Evaluation of the performances of these two topologies in terms of iron loss and torque (or output power) will be employed numerically, by means of finite element method (FEM) and the Flux2D software.

3.1. Integrated in-wheel motor magnetic gear topology

The considered in-wheel motor gear topology is the one presented in **Figure 8**. The motor is a fractional slot permanent magnet synchronous machine (FS-PMSM)—17 pairs of poles and 39 slots. Above the outer rotor of the FS-PMSM and attached to it, we have an inner rotor of the MG, having the same number of pairs of poles (p_{in}=17), and a reduced number of pairs of poles for the outer rotor of the MG (p_{out}=5). It means that the magnetic transmission will produce a higher speed, at a lower torque: it is a multiplier, or reversed gear [40]. Numerically computed results are shown in **Figures 10–12**.

Figure 10. Integrated motor-gear analyzed variant, based on in-wheel motor: field lines (left) and flux density distribution (right) within the active parts.
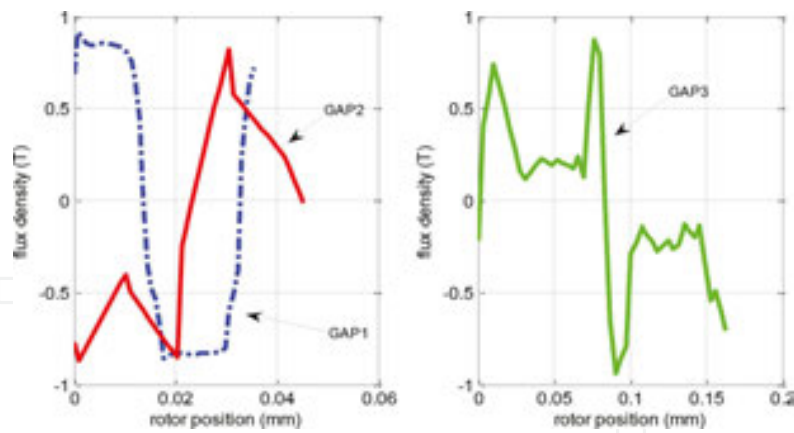
Figure 11. Air-gap flux density in the integrated motor-gear studied variant [40].
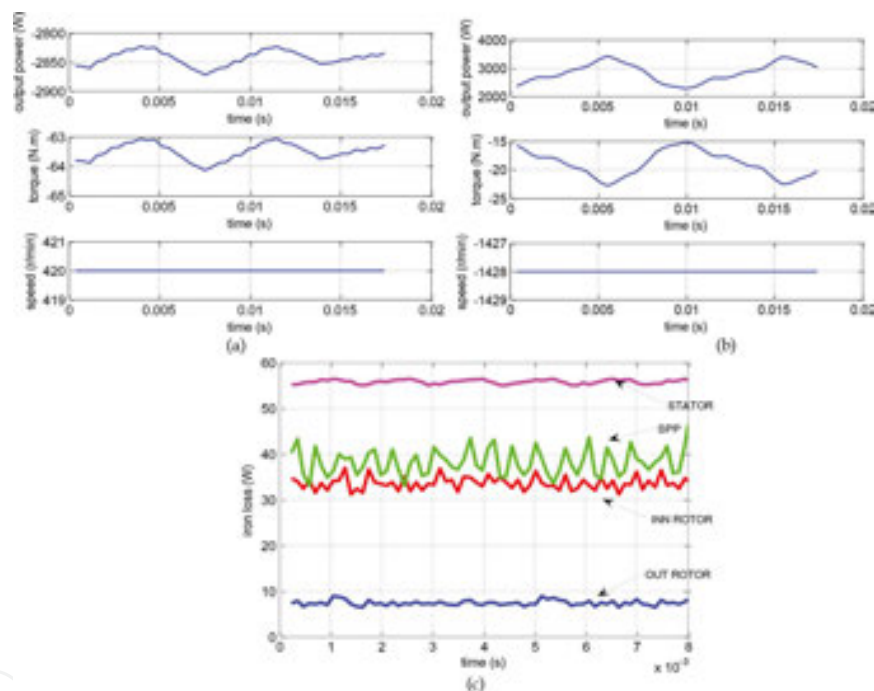

Figure 12. Performances of the integrated motor-gear studied variant: the speed-torque-power on the low speed rotor of the MG (a), for the high-speed outer rotor (b), and the iron loss in the active parts.

A first result of this analyzed integrated motor-gear variant is shown in **Figure 10**, where the field lines and flux density distribution within the active parts of the topology are presented. The reader can observe the influence of modulated teeth in the transfer of the flux (torque) from the inner to outer rotor. In the air gap layers of this machine-gear topology, the FEM software computed the following air gap flux densities, plotted in **Figure 11**: here, Gap1 refers to the in-wheel motor's air gap, Gap2 stands for the inner rotor air gap of the MG and Gap3 refers to its outer rotor air gap. More results are plotted in **Figure 12**.

The delivered torque and power, as well as the iron loss within the active parts of the integrated motor-gear studied variant are plotted in **Figure 11**. Some torque ripples can be identified, both on the inner and on the outer rotors of the integrated motor-gear variant. Since the major loss component within an MG is the iron loss, it is obvoius that the efficiency of the transmission is very low. One could sum the iron loss components (for the inner and outer rotor, as well as for the static part poles or teeth—SPP) and of the in-wheel motor to get 130 W. These results are not optimized. Based on the image of the flux density distribution (**Figure 10** right), we could consider to reshape the teeth's geometry and the outer rotor yoke, in the perspective of increasing the efficiency.

In order to prove the important advantage of MGs against classic mechanical gear, that is the possibility to obtain a very high transmission ratio for high-speed applications, and to get a very compact magnetic traction system with very good power density, the reader's attention will be oriented toward a high-speed MG.

3.2. MG with buried permanent magnets for high-speed applications

The second analyzed MG is with high-speed inner rotor, running at 26,000 r/min (with p_{in}=1), and outer rotor for low-speed rotor (with p_{out}=15) running at approximately 1500 r/min. The number of static part iron teeth is N_s=16. The magnets are buried in order to avoid the surface-mounted pieces which need a consolidating ring. A preliminary check on the mechanical resistance of the inner rotor steel needs to be employed numerically, to check if the iron bridges have not been damaged during MG's operation. A cross section of the high-speed MG is shown in **Figure 13**.
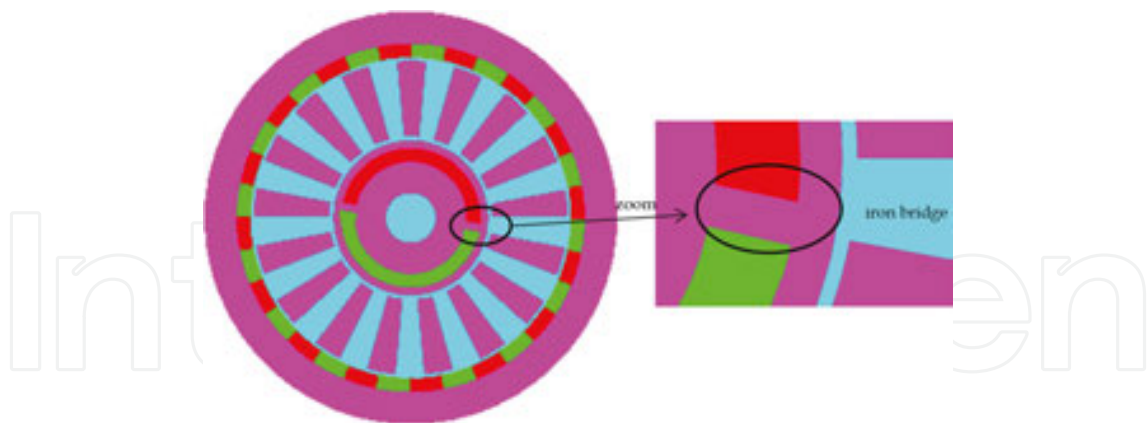

Figure 13. The high-speed MG studied variant.

This MG will be evaluated for different steel material characteristics (M335, M400, and Vacoflux48), and permanent magnet types (Nd-Fe-B, Ferrite, Alnico). As a reference variant, the MG with Nd-Fe-B and M400 steel is considered. The first result of this configuration is shown in **Figure 14**, where the field lines and flux density distribution are shown. An obvious saturation is found on the inner rotor core, on the iron's bridge, which is normal behavior since the flux needs to pass the air gap.
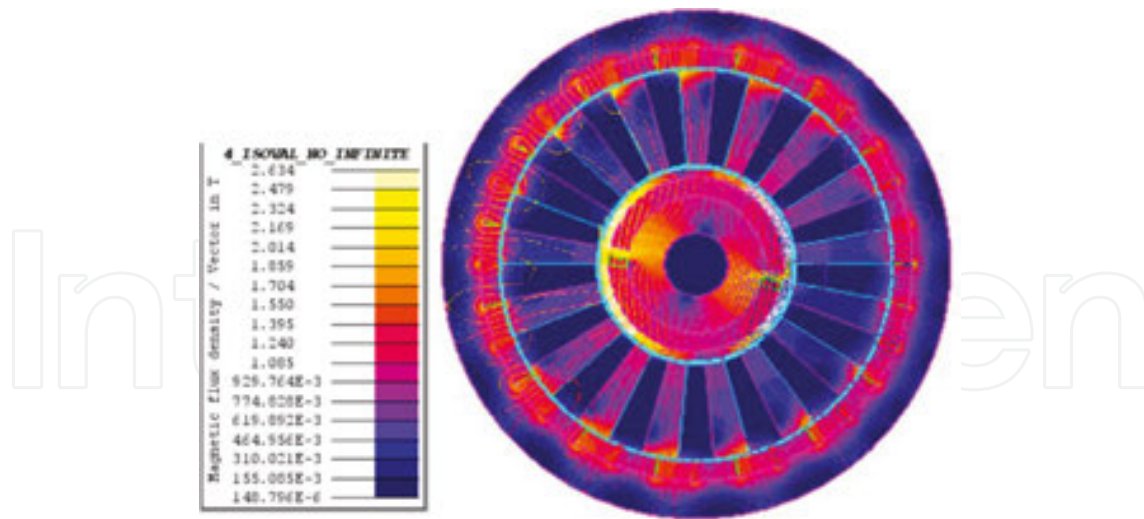
Figure 14. The field lines and flux density distribution within the active parts of the high-speed MG.

Some transient simulations were carried out in Flux2D. In **Figures 15–17** are presented the simulated results for the case of an MG with M400 steel used for all cores and armature, and Nd-Fe-b as magnet material. Here, the output power and torque as well as the iron losses in the active parts of the structure are plotted. Very smooth mechanical performances have been obtained with such configuration of MG, with 1/16 ratio. The amount of iron loss in this case is about 800 W.
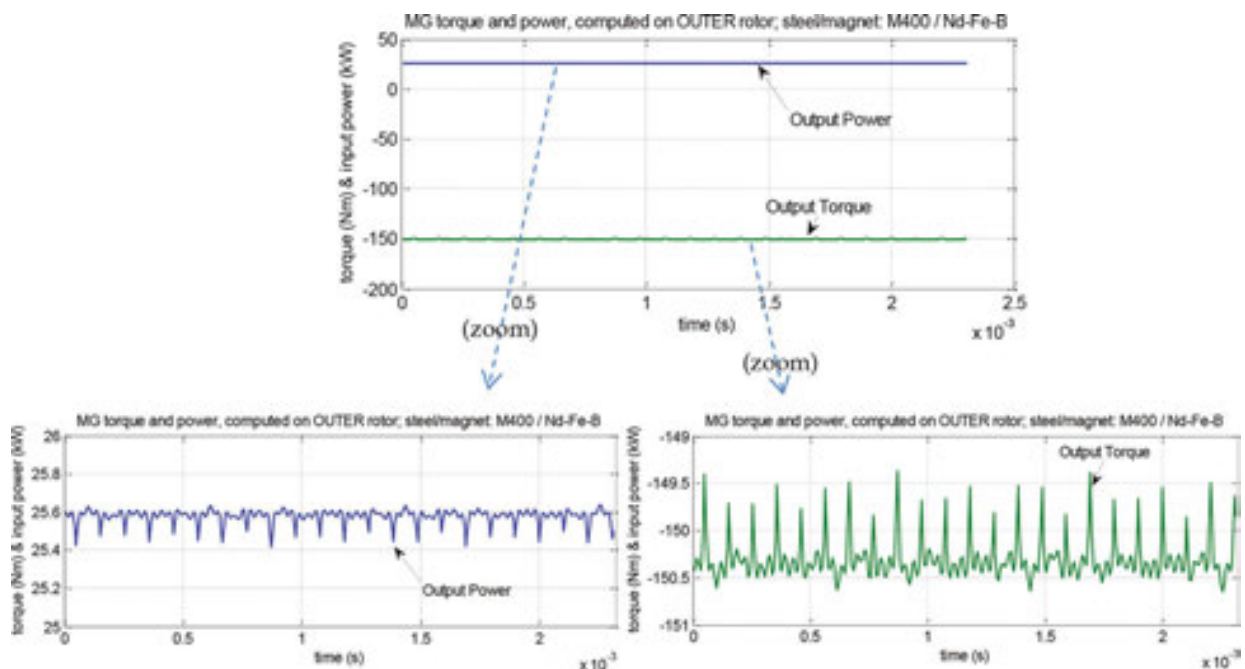
Figure 15. Simulated results for the MG with M400 steel and Nd-Fe-B magnet: input and output power [40].
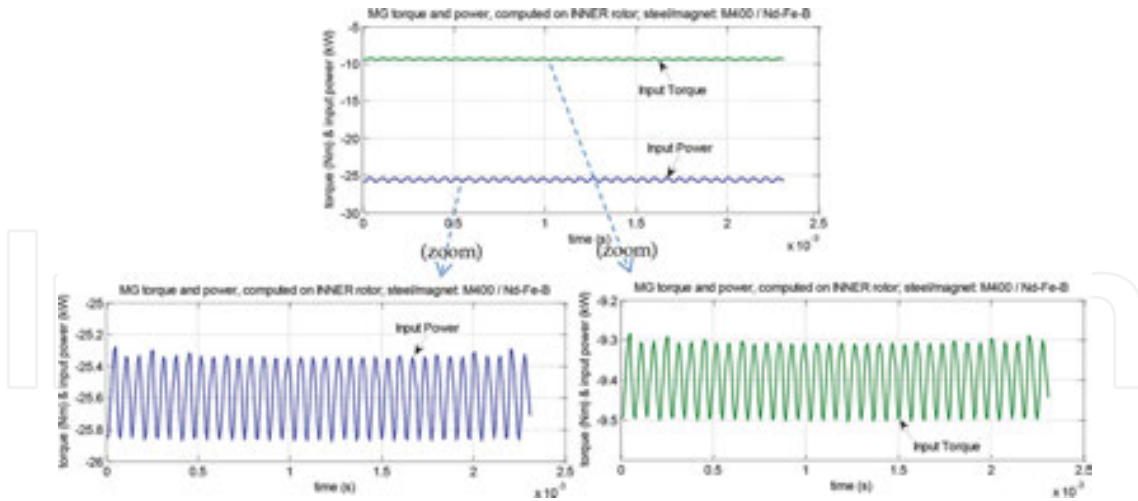
Figure 16. Simulated results for the MG with M400 steel and Nd-Fe-B magnet: input and output torque [40].
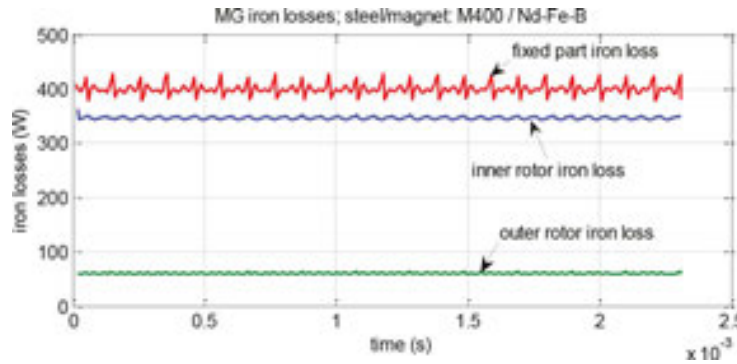

Figure 17. Simulated results for the MG with M400 steel and Nd-Fe-B magnet: iron losses in the active parts [40].

Now, let us see what happens if better material is used, such as the Vacoflux48 steel, which has a very narrow hysteresis curve. The iron loss results are given in **Figure 18**. (The mechanical output performances are not given here; only the amount of iron loss in the fixed iron teeth, inner, and outer rotor of the MG.)
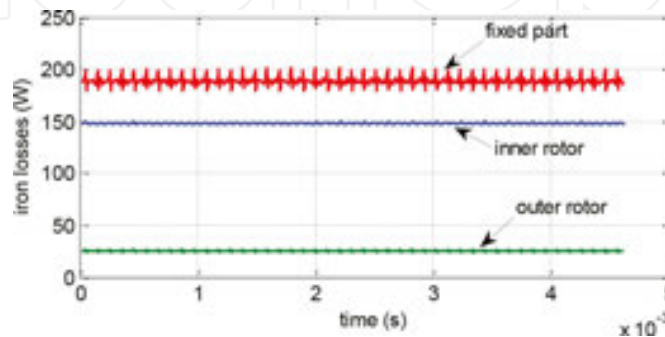

Figure 18. Simulated iron losses for the MG with Vacoflux48 steel and Nd-Fe-B magnet [40].

An amount of 365 W of iron loss was computed here. By comparing these iron losses (for the M400 steel, given in **Figure 17**, and the ones from **Figure 18**, for Vacoflux48), the huge advantage of the structure equiped with Vacoflux material is obvious, for which the iron loss is less than half of the M400—which is neither a bad material nor a cheap one. Of course, products based on Vacoflux48 are rather exclusive units and meant for special applications (like racing cars)—the cost of one prototype is almost prohibitively expensive. For ordinary applications, even the M400 steel is considered an expensive material—it is usually used for prototypes and low series manufacturing. Otherwise, a cheaper variant based on M335 is suitable in terms of output performances, giving similar results as the ones using M400.

A more complete comparison of the performances of the high-speed MG, when equipped with different types of materials and their magnetical characteristics is given in **Tables 4** and **5**—the width of the considered steel sheet (0.2, 0.35, and 0.5mm) is given also in **Table 4**.

Property	Material					
	PM			Steel		
	Nd-Fe-B	Alnico	Ferrite	M400 (0.5 mm)	M335 (0.35 mm)	Vacoflux48 (0.2 mm)
Remnant flux-density	1.35 T	1.27 T	0.45 T			
Relative magnetic permeability	1.05	1	16	~4000	~4000	~4000
Magnetic field intensity (coercivity at saturation)	−930 kA/m	−51.5 kA/m	−300 kA/m	50 kA/m	5 kA/m	1.9 kA/m
Saturation flux-density				2 T	1.6 T	2.25 T

Table 4. The properties of the materials used in the construction of the high-speed MG.

Materials	Parameter				
	T_{in} (Nm)	T_{out} (Nm)	Ripple of T_{in} (%)	Ripple of T_{out} (%)	Total Pfe (W)
Nd-Fe-B + M400	9.34	150.3	2.14	0.79	806.9
Alnico + M400	0.82	13.14	1.82	0.68	51.9
Ferrite + M400	0.637	10.18	3.3	0.98	22.9
Nd-Fe-B + M335	9.34	150.3	2.35	0.86	870
Nd-Fe-B + Vacoflux48	9.34	150.3	1.68	0.84	396.6

Table 5. Comparison of different configurations (material based) of MGs.

Some comments need to be made with respect to the Alnico and ferrite, the results of which are summarized in **Table 4**: for this specific configuration of the MG, because of the iron bridge which needs to support important centrifugal forces (we recall that the high-speed rotor is running at 26,000 r/min), and the low level of remanent flux density (for Ferrite material) or

coercivity (for Alnico), the magnetic flux is not sufficiently strong to cross the air gap. Different rotor configurations (with concentrated flux or halback array) need to be considered—which means that a topology with more than one pair of poles is requested. To prove this, one can investigate the field lines and the flux densities depicted in **Figure 16**, given within the active parts of the MG while ferrite or Alnico materials are used (**Figure 19**).
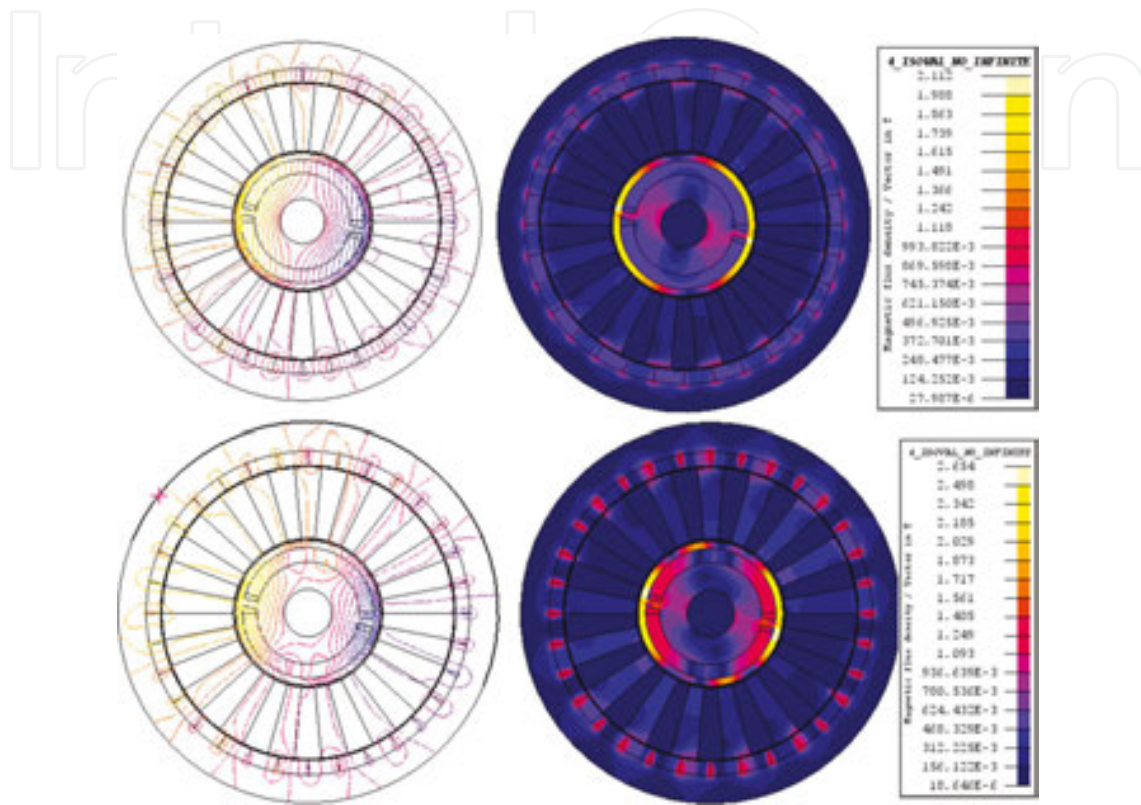

Figure 19. Investigation of the MG field lines and flux density distribution, when ferrite (top) and Alnico (bottom) magnets were considered.

As 15 years have passed since the first efficient MG proposition, we could expect, in the next years, improvements in the field of MGs, especially for the ones with variable transmission ratio, which could be extremely useful in transportation and aeronautical domains. With the advancement in the field of materials, for rare earth materials and ferromagnetic steel, the future of fully electromagnetic propulsion systems could be considered as a viable industrial solution, and not only a new research subject.

4. Conclusions

This chapter proposes an overview of the challenges in EV application, where the speed limits were pushed forward in the last decade. Practically, all the car manufacturers are proposing mobility solutions based on electrically propelled traction systems, which are limited because of the drawbacks of the mechanical gear, which needs to be continuously lubricated, presenting

important heat and local losses; moreover, higher speeds drastically decrease the power density of motorization. To overcome these drawbacks, researchers have proposed in the last decade possible solutions based on magnetic gears (MGs). We have presented in this chapter the existent configuration of fixed transmission ratio MGs, we have also indicated some references in which the variable transmission was studied and we have presented the main analytical approaches used for the design of MGs: the harmonic, magnetic reluctance equiv‐ alent circuit, and vector potential algorithms. A quasi-complete reference list was given with respect to this topic. Next, we have investigated two variants of MG, one with integrated motor and a second one for high-speed applications and a transmission ratio of 1/16. Through numerical computation we have investigated the output mechanical performances of the studied MGs, as well as the major loss component of such devices: the iron loss within the active parts of the MG. The influence of different materials on the active parts, meaning ferromagnetic steel and permanent magnets, was evaluated and a comparison of the obtained performances was depicted.

The research on MG has gained interest in the last decade and we expect that based on advancements in materials, the performances of these devices will be even more improved and will be of real interest, especially in the field of transportation and aeronautics.

Acknowledgements

Author details

Daniel Fodorean

Address all correspondence to: daniel.fodorean@mae.utcluj.ro

Faculty of Electrical Engineering, Department of Electrical Machines and Drives, Technical University of Cluj-Napoca, Cluj-Napoca, Romania

References

[1] A.E. Fuhs. Hybrid vehicle and the future of personal transportation. Boca Raton, Florida, USA: CRC Press, 2009.

[2] J. Larminie and J. Lowry. Electric vehicle technology explained. 2nd edition. West Sussex, England: Wiley, 2012.

[3] D. Fodorean, F. Jurca, M. Ruba, and D.C. Popa. Motorization variants for light electric vehicles – design, magnetic, mechanical and thermal aspects. Cluj-Napoca, Romania: AlmaMater June 2013.

[4] J. De Santiago, et al. Electrical motor drivelines in commercial all-electric vehicles: a review. IEEE Transactions on Vehicular Technology, vol. 61, no. 2, pp. 475–485, Feb. 2012.

[5] I. Husain. Electric and hybrid vehicles: design fundamentals. 2nd edition. Boca Raton, Florida, USA: CRC Press, 2011.

[6] M. Ehsani, Y. Gao, and A. Emadi. Modern electric, Hybrid electric, and Fuel cell vehicles: fundamentals, theory, and design – 2nd edition, CRC Press, Boca Raton, Florida, USA, 2010.

[7] C.W. Wessner. Building the U.S. battery industry for electric drive vehicles. The National Academies Press, USA, 2012.

[8] G. Pistoia. Electric and hybrid vehicles: power sources, models, sustainability, infra-structure and the market. Boca Raton, Florida, USA: CRC Press, 2010.

[9] R. James. Hendershot tutorial at ICEM conference, Berlin, 2–5 September, 2014: Electric Machine Design Strategies to Achieve IE2, IE3 & HEM (IE4) Efficiencies.

[10] 17th of June, 2016 http://www.osvehicle.com.

[11] D. Fodorean. Study of a high speed motorization with improved performances dedicated for an electric vehicle. IEEE Transactions on Magnetics, vol. 50, no. 2, Feb. 2014, paper no. 7022804.

[12] F. Luise, et al. Design and technology solutions for high-efficiency high-speed motors, ICEM 2012, Marseille, France, Sep. 2012, pp. 157–163.

[13] A. Tenconi, S. Vaschetto, and A. Vigliani. Electrical machines for high-speed applica-tions: design considerations and tradeoffs. IEEE Transactions on Industrial Electronics, vol. 61, no. 6, pp. 3022–3029, 2014.

[14] G. Pellegrino, A. Vagati, B. Boazzo, and P. Guglielmi. Comparison of induc-tion and PM synchronous motor drives for EV application including design examples. IEEE Transactions on Industry Applications, vol. 48, no. 6, pp. 2322–2332, Nov/Dec. 2012.

[15] D. Gerada, A. Mebarki, N.L. Brown, K.J. Bradley, and C. Gerada. Design aspects of high-speed high-power-density laminated-rotor induction machines. IEEE Transactions on Industrial Electronics, vol. 58, no. 9, pp. 4039–4047, Sept. 2011.

[16] K. Sung-Il, K. Young-Kyoun, L. Geun-Ho, and H. Jung-Pyo. A novel rotor configuration and experimental verification of interior PM synchronous motor for high-speed applications. IEEE Transactions on Magnetics, vol. 48, no. 2, pp. 995–998, 2012.

[17] D.P. Marcetic, I.R. Krcmar, M.A. Gecic, and P.R. Matic. Discrete rotor flux and speed estimators for high-speed shaft-sensorless IM drives. IEEE Transactions on Industrial Electronics, vol. 61, no. 6, pp. 3099–3108, June 2014.

[18] R.R. Moghaddam, F. Magnussen, and C. Sadarangani. Theoretical and experimental reevaluation of synchronous reluctance machine. IEEE Transactions on Industrial Electronics, vol. 57, no. 1, pp. 6–12, Jan. 2010.

[19] J.-H. Seo, T.-K. Chung, C.-G. Lee, S.-Y. Jung, and H-K. Jung. Harmonic iron loss analysis of electrical machines for high-speed operation considering driving condition. IEEE Transactions on Magnetics, vol. 45, no. 10, pp. 4656–4659, Oct. 2009.

[20] K. Atallah and D. Howe. A novel high-performance magnetic gear. IEEE Transactions on Magnetics, vol. 37, no. 4, pp. 2844–2845, Jul. 2001.

[21] M. Aubertin, A. Tounzi, and Y. Le Mach. Study of an electromagnetic gearbox involving two permanent magnet synchronous machine using 3-D-FEM. IEEE Transactions on Magnetics, vol. 44, no. 11, pp. 4381–4384, Nov. 2008.

[22] M. Fukuoka, K. Nakamura, and O. Ichinokura. Dynamic analysis of planetary type magnetic gear based on reluctance network analysis. IEEE Transactions on Magnetics, vol. 47, no. 10, pp. 2414–2417, Oct. 2011.

[23] E. Gouda, S. Mezani, L. Baghli, and A. Rezzoug. Comparative study between mechanical and magnetic planetary gears. IEEE Transactions on Magnetics, vol. 47, no. 2, pp. 439–450, Feb. 2011.

[24] D. Fodorean. Magnetic gear with transmission ration in steps (original title in Romanian) – patent proposal, A/00869/17.11.2014.

[25] J. Rens, R. Clark, S. Calverley, K. Atallah and D. Howe. Design, analysis and realization of a novel magnetic harmonic gear. In: Proceedings of the 2008 International Conference on Electrical Machines Paper ID 1454, Villamoura, Portugal, 2008.

[26] Linni Jian, Guoqing Xu, Chunting Chris Mi, K.T. Chau, and C.C. Chan. Analytical method for magnetic field calculation in a low-speed permanent-magnet harmonic machine. IEEE Transactions on Energy Conversion, vol. 26, no. 3, pp. 862–870, Sept. 2011.

[27] F.T. Jørgensen, T.O. Andersen, and P.O. Rasmussen. The cycloid permanent magnetic gear. IEEE Transactions on Industry Applications, vol. 44, no. 6, pp. 1659–1665, Nov/Dec. 2008.

[28] T. Lubin, S. Mezani, and A. Rezzoug. Development of a 2D analytical model for the electromagnetic computation of axial-field magnetic gears. IEEE Transactions on

Magnetics, Institute of Electrical and Electronics Engineers, 2013, DOI: 10.1109/TMAG. 2013.2267746.

[29] Mu Chen, Kwok-Tong Chau, Christopher H. T. Lee, and Chunhua Liu, Design and analysis of a new axial-field magnetic variable gear using pole-changing permanent magnets. Progress in Electromagnetics Research, vol. 153, pp. 23–32, 2015.

[30] Linni Jian, K.T. Chau, and J.Z. Jiang, An integrated magnetic-geared permanent magnet in-wheel motor drive for electric vehicles. IEEE Vehicle Power and Propulsion Conference (VPPC), September 3–5, 2008, Harbin, China.

[31] P.O. Rasmussen, H.H. Mortensen, T.N. Matzen, T.M. Jahns, and H.A. Toliyat. Motor integrated permanent magnet gear with a wide torque-speed range. IEEE Energy Conversion Congress and Exposition, 2009. ECCE 2009, 20–24 September 2009, San Jose, California, USA. pp. 1510–1518.

[32] D. Fodorean, C. Irimia, and P. Minciunescu. Performances evaluation of a magnetic gear with high transmission ratio used for high speed applications, Progress in Electromagnetics Research Symposium, Prague, Czech Republic, 06–09 July, 2015, pp. 627–631.

[33] D. Fodorean. Study of a high speed motorization with improved performances dedicated for an electric vehicle. IEEE Transactions on Magnetics, vol. 50, no. 2, paper no. 7022804, Feb. 2014.

[34] P. Rasmussen, T. Andersen, F. Jorgensen, and O. Nielsen. Development of a high-performance magnetic gear. IEEE Transactions on Industry Applications, vol. 41, no. 3, pp. 764–770, May/June 2005.

[35] Yi-Chang Wu and Chih-Wen Wang. Transmitted torque analysis of a magnetic gear mechanism with rectangular magnets. Applied Mathematics & Information Sciences, vol. 9, no. 2, pp. 1059–1065, 2015.

[36] K. Atallah, S.D. Calverley, and D. Howe. Design, analysis and realisation of a high performance magnetic gear. IEEE Proceedings-Electric Power Applications, vol. 151, no. 2, pp. 135–143, Mar 2004.

[37] L. Jian and K. T. Chau. Analytical calculation of magnetic field distribution in coaxial magnetic gears. Progress in Electromagnetics Research, PIER 92, pp. 1–16, 2009.

[38] K. Nakamura, M. Ishihara, and O. Ichinokura. Reluctance network analysis model of a permanent magnet generator considering an overhang structure and iron loss, ICEM 2006, Chania, Greece, paper no. 311, September 2006.

[39] L. Jian and G. Xu. Electromagnetic design and analysis of a novel magnetic-gear-integrated wind power generator using time-stepping finite element method. Progress in Electromagnetics Research, vol. 113, pp. 351–367, 2011.

[40] C.V. Pop and D. Fodorean. In-wheel motor with integrated magnetic gear for extended speed applications. IEEE SPEEDAM 2016, Capri, Italy, 22–24 June 2016, accepted for publication.

[41] T. Lubin, S. Mezani, and A. Rezzoug. Analytical computation of the magnetic field distribution in a magnetic gear. IEEE Transactions on Magnetics, Institute of Electrical and Electronics Engineers, vol. 46, no. 7, pp. 2611–2621, 2010.